JCTC Journal of Chemical Theory and Computation

Chemical Detail Force Fields for Mesogenic Molecules

Ivo Cacelli, Antonella Cimoli, Luca De Gaetani, Giacomo Prampolini, and
Alessandro Tani*

*Dipartimento di Chimica e Chimica Industriale, Università di Pisa,
via Risorgimento 35, I-56126 Pisa, Italy*

Abstract: Intra- and intermolecular potential energy surfaces of the 4,4′-di-*n*-heptyl azoxyben-zene molecule have been sampled by *ab initio* calculations and represented through a force field suitable for classical bulk simulations. The parametrization of the molecular internal flexibility has been performed by a fitting procedure based on single molecule Hessian, gradients and torsional energies, computed using density functional theory. The intermolecular part of the force field has been derived as a pure pair potential, by fitting the dimer potential energy surface sampled by the Fragmentation Reconstruction Method. Preliminary molecular dynamics runs have been performed on systems of 210 and 600 molecules at atmospheric pressure and different temperatures, showing the presence of ordered and isotropic phases. Several properties have been computed, all resulting in a good agreement with the corresponding experimental data.

1. Introduction

Molecular dynamics (MD) simulations[1,2] have rapidly become a powerful tool in the study of soft matter.[3-6] The massive increase of computational resources has nowadays made possible performing molecular dynamics (MD) atomistic simulations on bulk phases up to thousands of medium sized molecules for several tens of nanoseconds. At the same time, there has been a growing effort to search for "realistic" force fields (FF), capable of retaining most of the detail which specifies the chemical identity of the bulk phase forming molecules. One possibility is to adopt a FF parametrization based on quantum mechanical (QM) calculations[7] on both monomer and dimer of the target molecule. This *ab initio* derived (ABD) model potential can then be employed in MD simulations for the calculation of the bulk properties. A scheme of such approach can be summarized as follows:

1) QM calculations of intermolecular and intramolecular potentials with quantum mechanical methods

2) Parameterization of the computed energies (and possibly, energy derivatives) with an analytical model potential suitable for computer simulations

3) MD simulations and comparison of the resulting macroscopic properties with the relevant experimental data

QM based parametrizations of the intramolecular FF part have been proposed by several groups and employed in widely used force fields.[8-14] In a recent work,[15] parameters for bonded interactions and partial charges of the azobenzene group (AB) have been derived from *ab initio* molecular dynamics reference calculations. A classical FF, including this description of the AB unit, was applied to the liquid crystal 8AB8, where 8-carbon chains are linked to the phenyl rings of AB via ether bonds. However, the phase transition temperatures were missed by almost 100 K.

In this paper, the equilibrium internal coordinates and the force constants of the HAB molecule are obtained by fitting DFT optimized energies, gradients and Hessian matrix using the JOYCE[16] program, recently[17] developed in our laboratory.

The QM route to intermolecular FF is much more involved because it requires the creation of a large energy vs geometry database, obtained by suitable post Hartree−Fock calculations capable of capturing a relevant fraction of the correlation energy, in order to properly account for the dispersion energy. Moreover, from early simulations on liquid argon[1] and argon−krypton mixtures,[18] it was found that the inclusion of three-body interactions in the intermolecular potential is a necessary condition to obtain accurate results of pressure and liquid−vapor equilibria.

* Corresponding author e-mail: tani@dcci.unipi.it.

Unfortunately, the inclusion of three-body interactions in the QM database as well as in the MD simulation, is computationally prohibitive in view of the dimensions of the molecules that typically can form mesophases. On the other hand, it has been demonstrated that the use of standard FFs, based on two-body effective potentials that include three-body effects in an average way, does not lead to accurate results in the case of liquid crystal forming molecules.[19] However, in a previous work on benzene,[20] we have shown that an accurate two-body potential is capable of accounting for several bulk properties, both in crystalline and liquid phases. The overall performance of that ABD FF was comparable to that obtained by employing the well-known OPLS effective potential,[21] which was tuned to reproduce experimental density and vaporization enthalpy of liquid benzene. In the case of larger molecules, e.g. polymers or liquid crystals, a corresponding tuning of the FF parameters can be very time-consuming for the long equilibration time, and this route is rather hard to be pursued.[19] On the other hand, the transferability of such parameters from smaller molecules does not allow for retaining a sufficient degree of chemical specificity. Moreover, FF parameters are tuned for a well-defined thermodynamic state (usually the isotropic liquid), so it is unlikely that their quality stays the same in different thermodynamic conditions.

For these reasons in this paper we neglect three-body effects and consider only two-body intermolecular interactions. Even with this reduction, a reliable QM sampling of a dimer potential energy surface (PES) is very computational demanding for the large number of dimer arrangements to be considered. For this step, we employ the Fragmentation Reconstruction Method (FRM),[7,22] which allows us to calculate the dimer intermolecular energies of large molecules with reduced effort, while preserving high accuracy. This method is based on fragmenting each monomer into moieties and reconstructing the intermolecular energy as a sum of the interaction energies of all pairs of resulting fragments (see Section 3.2).

In previous applications on medium size molecules, the indirect reconstruction route of FRM was adopted for *n*-pentyl-4′-cyanobiphenyl (5CB),[22,23] while the direct route was followed for *n*-pentyloxy-4′-cyanobiphenyl (5OCB)[17] (see the following section for details). The MD results obtained for 5CB and 5OCB seem to indicate that closer agreement with the experimental data is obtained if the potential is parametrized through the direct route. In fact, the overall behavior of the 5CB intermolecular model FF appeared to be slightly too attractive, resulting in an overestimation of the density by almost ∼6%,[23] which was shown to have dramatic effects on the translational dynamics.[24] On the other hand, when the direct reconstruction is employed, as for 5OCB, the density is much better reproduced (∼2%) and, consequently, a more accurate description of the translational dynamics is achieved.[17]

We believe additional tests of our approach to force fields are in order, to prove that it is worth the extra computational effort it entails, compared to the straightforward use of literature potentials.

In this paper a new application of the FRM is proposed for the mesogenic molecule 4,4′-di-*n*-heptylazoxybenzene (HAB) via the direct method for the parametrization of the intermolecular FF. HAB can be considered a good test case, as its molecule contains new chemical motifs that force us to explore diverse fragmentation schemes. In addition, its smectic phase has a reasonably large range of stability, although this is not true for the nematic one. The fairly large amount of experimental data available on HAB (see e.g. ref 25) provide the necesssary information for a thorough test of our model force field.

A successful validation, obtained from a detailed calculation of several relevant experimental observables, would support the reliability of the approach, confirming the possibility of exploiting its predictive capabilities in the calculations of properties not easily accessible to experiments and/or of not yet synthesized materials.

The paper is organized as follows: Section 2 contains the main computational details of both QM and MD calculations; the results of the FF parametrization are reported in Section 3, together with the discussion of preliminary simulation runs. Main conclusions are collected in the last section.

2. Methods and Computational Details

2.1. Intramolecular FF. QM calculations for both intra- and intermolecular PES sampling were performed with the GAUSSIAN 03 package.[26] In all single molecule calculations, the density functional B3LYP method[27] was used with a correlation consistent basis set, cc-pvDz. The absolute energy minimum was obtained by a complete geometry optimization. Vibrational frequencies, gradients and Hessian matrix were computed only for this conformation. Energy profiles for flexible dihedrals were obtained by performing geometry optimizations without any restriction but the investigated torsional angle, which is increased in a stepwise manner. The torsional energy fitting was performed within the Frozen Internal Rotation Approximation.[28]

From this database, the intramolecular FF has been parametrized with the JOYCE program,[16] through a least-squares minimization of the functional I^{intra}

$$I^{intra} = \sum_{g=0}^{N_{geom}} W_g [U_g - E_g^{intra}]^2 + \sum_{K \le L}^{3N-6} \frac{2W''_{KL}}{(3N-6)(3N-5)} \times \left[H_{KL} - \left(\frac{\partial^2 E^{intra}}{\partial Q_K \partial Q_L} \right) \right]_{g=0}^2 \quad (1)$$

where N_{geom} is the number of the sampled conformations, Q_K is the Kth normal coordinate, and U_g is the DFT computed energy in the gth geometry. The QM Hessian matrix H_{KL} and the FF Hessian are evaluated at the absolute minimum $g = 0$. Two different weights W_g have been chosen: 0.0076 for the conformations with a low internal energy ($\simeq 5$ kJ/mol) and 0.0019 for all the others, in order to obtain a more accurate description of the more lowest energy geometries. The diagonal and off diagonal elements of the weight matrix W'' were set to 0.05 Å^4 amu^2 and 0.025 Å^4 amu^2, respectively. Details of the fitting procedure can be found in ref 28.

The employed intramolecular ABD-FF E^{intra} is in diagonal form (i.e., without coupling terms between internal coordinates)

$$E^{intra} = E^{stretch} + E^{bend} + E^{Rtors} + E^{Ftors} + E^{LJintra} \tag{2}$$

The first three terms have an harmonic expression

$$E^{stretch} = \frac{1}{2} \sum_{\mu}^{N_s} k_{\mu}^s (r_{\mu} - r_{\mu}^0)^2; \quad E^{bend} = \frac{1}{2} \sum_{\mu}^{N_b} k_{\mu}^b (\theta_{\mu} - \theta_{\mu}^0)^2;$$

$$E^{Rtors} = \frac{1}{2} \sum_{\mu}^{N_{Rt}} k_{\mu}^t (\phi_{\mu} - \phi_{\mu}^0)^2 \tag{3}$$

where k_{μ}^s, k_{μ}^b, k_{μ}^t and r_{μ}^0, θ_{μ}^0, ϕ_{μ}^0 are the force constants and equilibrium values for stretching, bending, and rigid torsional internal coordinates, respectively. For flexible dihedrals a sum of cosines is used, namely

$$E^{Ftors} = \sum_{\mu}^{N_{Fdihedrals}} \sum_{j=1}^{N_{\mu}} k_{j\mu}^d [1 + \cos(n_{\mu}^j \delta_{\mu} - \gamma_{\mu}^j)] \tag{4}$$

where $k_{j\mu}^d$ is the force constant, δ_{μ} is the flexible dihedral, and n_{μ}^j and γ_{μ}^j are the multiplicity and a phase factor for the jth cosine. N_{μ} is the number of cosine functions employed for dihedral μ. Finally, in the last term of eq 2, $E^{LJintra}$ is the standard 12−6 Lennard-Jones potential between the interaction sites of the same molecule.

2.2. Intermolecular FF. As mentioned above, the FRM approach can be implemented in an indirect and a direct way. In both cases, the molecules of the target dimer are fragmented into the same number of moieties. In the indirect approach the PES of all resulting fragment-fragment pairs were computed at the QM level for many geometrical arrangements. All PESs were fitted with complex site−site analytical model functions[22] including several polynomials, exponentials, and Gaussian functions, with and without angular dependence. The intermolecular PES of the target dimer was eventually reconstructed by summing up all the fragment-fragment analytical model functions. It must be stressed that only during the reconstruction step the fragments are arranged in the same geometry in which they are reciprocally placed when considered as moieties of the whole molecules.

Conversely, in the direct FRM route, the fitting step of the fragment-fragment PES is avoided, and the sampling procedure is directly performed on the whole dimer. For each dimer arrangement, the interaction energy is computed at the QM level by summing the appropriate fragment-fragment contributions obtained by QM calculation, rather than summing the energy contribution obtained by previous fragment-fragment fittings, as in the indirect route.

Here, the HAB intermolecular PES was sampled through FRM,[7,22] computing the fragment-fragment interaction energies of all dimers with the direct route, in the supermolecule approach with a MP2 method, and considering the BSSE by the standard counterpoise correction.[29] A suitably 6-31G* modified basis set was used, where the exponents of the d polarization functions are decreased to $\alpha_d = 0.25$, following the suggestion of Hobza and co-workers.[30,31] As to the

benzene dimer, which can be considered as a prototype for the aromatic interactions, the interaction energies computed at the MP2/6-31G*(0.25) level were shown[20,30,31] to well reproduce the results of high quality calculations.[32,33] In our case, the results of former FRM applications[20,22,34−36] suggest that this choice is a good compromise between the accuracy required in the PES description and the high number of energies required for an accurate sampling.

The intermolecular parameters were obtained from a least-squares fitting procedure, by minimizing the functional

$$I^{inter} = \frac{\sum_{k=1}^{N_{geom}} [(U_k^{FRM} - E_k^{inter})^2] e^{-\alpha U_k^{FRM}}}{\sum_{k=1}^{N_{geom}} e^{-\alpha U_k^{FRM}}} \tag{5}$$

where N_{geom} is the number of geometries considered for the HAB dimer, U_k^{FRM} is the energy of the kth dimer arrangement computed by FRM/MP2, and E_k^{inter} is the value of the fitting model function for the geometry k

$$E_k^{inter} = \sum_{i=1}^{N_{sites}} \sum_{j=1}^{N_{sites}} [E_{ij}^{LJ} + E_{ij}^{Coul}]_k \tag{6}$$

where E_{ij}^{LJ} and E_{ij}^{Coul} are the standard 12−6 Lennard-Jones potential and the charge−charge interaction between a pair of sites i,j of two different molecules. As for other applications,[7,20] the minimization procedure of functional I^{inter} was performed by imposing for all geometries a Boltzmann-like weight with $\alpha = 1.6$ kJ/mol^{-1}.

2.3. Bulk Simulations. The ABD-FF, obtained as sketched above, has been employed for preliminary MD simulations carried out with a parallel version of the Moscito4.0[37] package on systems of 210 and 600 HAB molecules. In all runs bond lengths were kept fixed at their equilibrium value using the SHAKE algorithm[38] which allowed us to use a time step of 2 fs. Charge−charge long-range forces were treated with the particle mesh Ewald method,[39,40] using a convergence parameter α of $5.36/2R_c$ and a 4th order spline interpolation, while the short-range interactions were truncated at $R_c = 10$ Å, employing standard corrections for energy and virial.[1] In the NPT ensemble, temperature and pressure were kept constant using the weak coupling scheme of Berendsen et al.[41]

The equilibration of the resulting trajectories was assessed by monitoring the mass density (ρ), the positional and orientational order vs the simulation time. The phase director **n** was identified as the eigenvector corresponding to the largest eigenvalue of the Saupe ordering matrix $\hat{\mathbf{Q}}$, whose elements are

$$Q_{ab} = \left\langle \frac{1}{2}(3u_a u_b - \delta_{ab}) \right\rangle$$

where the mean value $\langle ... \rangle$ is obtained averaging on all molecules composing the system, and **u** (a = x,y,z) is the unit vector of HAB molecular long axis. The orientational order was measured through the second rank order parameter P_2, computed as the maximum eigenvalue of $\hat{\mathbf{Q}}$. Positional
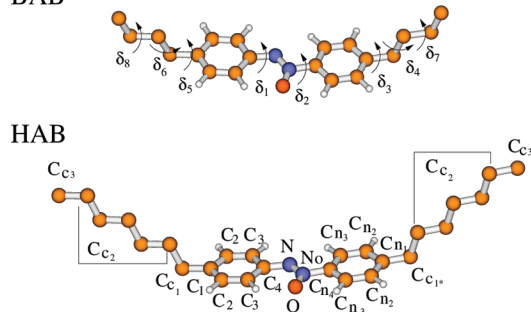
BAB

HAB

Figure 1. Model adopted for the HAB molecule (bottom panel) and flexible dihedral definition in the BAB homologue, employed for intramolecular parametrization (top panel). All aromatic hydrogens have been labeled after the carbon atom they belong to, i.e. H_{n3} is hydrogen bonded to the C_{n3} atom, etc.

order was monitored by computing the positional order parameter τ

$$\tau = \left\langle \left| \exp\left(2\pi i \frac{\mathbf{r} \cdot \mathbf{e}}{d}\right) \right| \right\rangle \tag{7}$$

where $\mathbf{r}$ is the position of the molecular center of mass, $\mathbf{e}$ is the unit vector normal to the smectic layers, and d is the layer separation. The latter is unknown and is optimized in order to maximize τ, since this ensures that the average we obtain has the same periodicity as the translational distribution function.[42]

Once equilibrated, HAB systems at several temperatures were simulated in the NVE ensemble to calculate some dynamical properties, as the isotropic translational diffusion coefficient D and the shear viscosity η_S. The former is computed as proportional to the long time limit of the center of mass mean square displacement (MSD)

$$D = \lim_{t \to \infty} D(t) = \lim_{t \to \infty} \frac{1}{6t} \langle [r(t) - r(0)]^2 \rangle \tag{8}$$

where $\langle ... \rangle$ means a double average over all configurations and molecules. The shear viscosity is computed as

$$\eta_S = \lim_{t \to \infty} \frac{V}{6k_B T} \int_0^t C_o(t') dt' \tag{9}$$

where V is the volume of the simulation box, k_B is the Boltzmann constant, and $C_o(t')$ is the correlation function of the off-diagonal elements of the stress tensor $\hat{\boldsymbol{\sigma}}$.[43] Due to the long time scales that characterize the collective dynamics of these systems, it has been necessary to extrapolate the value of η_S from a fitting with a double exponential function, as done previously in other applications.[24]

3. Results and Discussion

3.1. Intramolecular Parametrization. The HAB molecule is described with a full atomic model, except for the aliphatic hydrogens which are grouped with the chain carbon they are bonded to, in a united atom (UA) description, for a total of 37 interaction sites per molecule (see Figure 1).

Table 1. BAB: Optimized Stretching Parameters

		stretching			
bond	r_0 (Å)	k^s (kJ/(mol Å²))	bond	r_0 (Å)	k^s (kJ/(mol Å²))
C_{c1}-C_1	1.511	2699	C_{c1^*}-C_{n1}	1.512	2699
C_1-C_2	1.403	2766	C_{n2}-C_{n1}	1.405	2766
C_2-C_3	1.392	3377	C_{n3}-C_{n2}	1.394	3377
C_3-C_4	1.415	3083	C_{n3}-C_{n4}	1.397	3083
C_2-H_2	1.093	3368	C_{n2}-H_{n2}	1.093	3368
C_3-H_3	1.087	3368	C_{n3}-H_{n3}	1.088	3368
C_4-N	1.400	2841	C_{c3}-C_{c2}	1.530	2644
N-N_O	1.281	4124	C_{c1}-C_{c2}	1.541	2308
N_O-O	1.254	3960	C_{c1^*}-C_{c2}	1.541	2308
N_O-C_{n4}	1.467	1925	C_{c2}-C_{c2}	1.532	2308

The intramolecular contribution to the FF, E^{intra}, was parametrized on an HAB smaller homologue, namely 4,4′-dibutylazoxybenzene (BAB, see Figure 1), which differs from the target molecule for six methylene units (three for each side chain). This seemed a reasonable choice since it reduces the computational time and the UA parameters describing the flexibility of the longer chains (HAB) are not expected to be much different from those obtained for the smaller homologue (BAB).

The internal coordinates can be classified into flexible and rigid ones. Rigid coordinates are bond lengths, bond angles, and those dihedral angles determining the aromatic ring planarity, and they are all described with the harmonic type potential reported in eq 3. Conversely dihedrals δ_1-δ_8 reported in Figure 1 are to be considered flexible coordinates: the harmonic approximation fails in describing their potential, since the energy profile allows them to assume several values between 0° and 360° at room temperature and they will be described through the cosine expansion (4). Among these, δ_1 is the angle between the aromatic ring bonded to the site labeled N and the azoxy bridge plane; δ_2 is the analogue of δ_1 referred to the other ring; δ_3 and δ_5 are the angles formed by the aromatic ring plane and the plane containing the first two atoms of the aliphatic chain. Finally, δ_4 and δ_6-δ_8 are the dihedral angles driving the flexibility of the aliphatic chains. The Hessian matrix for the BAB minimum energy conformation has been computed together with the torsional energy profile for dihedrals δ_1 to δ_6, which have been sampled with steps of 30° in the [0−180] range.

No sampling has been performed for δ_7 and δ_8, and their description was made through the parameters reported for *n*-butane,[9] assuming the transferability of this torsional potential. Thus, the JOYCE fitting procedure was applied according to eq 1, with $N_{geom} = 42$, yielding an overall standard deviation of 0.044 kJ/mol, with maximum error on energies of 1.7 kJ/mol (optimized parameters are reported in Tables 1−4).

The torsional profile for δ_1-δ_8 is reported in Figure 2 which shows the very good agreement between the DFT computed energies and the ABD torsional curves. The lowest energy of δ_1 and δ_2 is at 0° with a torsional barrier of ~25 kJ/mol at 90° meaning that in the equilibrium geometry the azoxy group and the aromatic rings are expected to be coplanar. On the contrary, δ_3 and δ_5 prefer a 90° conformation, as found at the aliphatic-aromatic linkage in more simple compounds as ethylbenzene.[44] The energy profile vs both

Table 2. BAB: Optimized Bending Parameters

Bending					
Angle	θ_0 (°)	k^b (kJ/(mol·rad^2))	Angle	θ_0 (°)	k^b (kJ/(mol·rad^2))
$C_{c1}C_1C_2$	121.2	896.7	$C_{c1*}C_{n1}C_{n2}$	120.9	896.7
$C_1C_{c1}C_{c2}$	113.2	760.6	$C_{n1}C_{c1*}C_{c2}$	113.1	760.6
$C_2C_1C_2$	117.7	449.5	$C_{n2}C_{n1}C_{n2}$	118.0	434.1
$C_1C_2C_3$	122.3	434.1	$C_{n1}C_{n2}C_{n3}$	121.5	434.2
$C_2C_3C_4$	119.6	968.7	$C_{n2}C_{n3}C_{n4}$	118.9	968.8
$C_3C_4C_3$	118.1	245.2	$C_{n3}C_{n4}C_{n3}$	121.0	245.2
$C_1C_2H_2$ $C_3C_2H_2$ $C_2C_3H_3$ $C_4C_3H_3$	120.0	317.5	$C_{n1}C_{n2}H_{n2}$ $C_{n3}C_{n2}H_{n2}$ $C_{n2}C_{n3}H_{n3}$ $C_{n4}C_{n3}H_{n3}$	120.0	317.5
C_3C_4N	120.0	431.0	$N_OC_{n4}C_{n3}$	120.0	666.5
C_4NN_O	121.2	785.2	NN_OC_{n4}	115.1	103.6
NN_OO	128.0	705.2	$C_{n4}N_OO$	116.9	757.0
$C_{c3}C_{c2}C_{c2}$	113.2	836.9	$C_{c2}C_{c2}C_{c3}$	113.1	836.9
$C_{c1*}C_{c2}C_{c2}$	113.2	836.9	$C_{c1}C_{c2}C_{c2}$	113.3	836.9

Table 3. BAB: Optimized Rigid Torsion Parameters

Rigid torsions					
Dihedral Angle	ϕ_0 (°)	k^t (kJ/(mol·rad^2))	Dihedral Angle	ϕ_0 (°)	k^t (kJ/(mol·rad^2))
$C_{c1}C_1C_2C_3$	180.0	100.4	$C_{c1*}C_{n1}C_{n2}C_{n3}$	180.0	100.4
$C_{c1}C_1C_2H_2$	0.0	59.05	$C_{c1*}C_{n1}C_{n2}H_{n2}$	0.0	59.05
$C_2C_1C_2C_3$ $C_1C_2C_3C_4$ $C_2C_3C_4C_3$	0.0	87.54	$C_{n2}C_{n1}C_{n2}C_{n3}$ $C_{n1}C_{n2}C_{n3}C_{n4}$ $C_{n2}C_{n3}C_{n4}C_{n3}$	0.0	87.54
$C_2C_1C_2H_2$ $C_1C_2C_3H_3$ $C_4C_3C_2H_2$ $C_3C_4C_3H_3$	180	65.37	$C_{n2}C_{n1}C_{n2}H_{n2}$ $C_{n1}C_{n2}C_{n3}H_{n3}$ $C_{n4}C_{n3}C_{n2}H_{n2}$ $C_{n3}C_{n4}C_{n3}H_{n3}$	180	65.37
$H_2C_2C_3H_3$	0.0	36.16	$H_{n2}C_{n2}C_{n3}H_{n3}$	0.0	36.16
$C_2C_3C_4N$	180.0	30.18	$C_{n2}C_{n3}C_{n4}N_O$	180.0	189.1
$H_3C_3C_4N$	0.0	59.22	$H_{n3}C_{n3}C_{n4}N_O$	0.0	59.22
C_4NN_OO	0.0	222.5	$C_4NN_OC_{n4}$	180.0	248.7

chain dihedrals, δ_4 and δ_6, has an absolute minimum at 180° (*trans* conformation) and a relative one at ±60° *gauche* conformations) separated by rather high barriers. It is worth noticing that, as expected, the torsional potential curves of the chain dihedrals δ_4 and δ_6 are in excellent accord with those of *n*-butane (see Figure 2), confirming that this potential can be confidently transferred to all aliphatic chain dihedrals.

Extending the fitted intramolecular potential to the HAB molecule is now straightforward: by looking at the bottom panel of Figure 2 it is clear that all the inner chain dihedrals behave in similar manner, since the fitted torsional profile for δ_4 and δ_6 exactly traces out the δ_7, δ_8 shape, which is transferred from *n*-butane.

A fortiori, the force constants of more rigid internal coordinates, as methylene-methylene bond stretching and angle bending, are also expected to be transferable from those computed for the BAB smaller chains.

However, some intramolecular LJ terms were added to the FF. Previous experience on the UA modeling of 5CB molecule[23] stressed the need for such terms to both prevent an unphysical curling of the aliphatic chain on the core and on itself and to correctly take into account intramolecular interaction between the aromatic carbons and the methyl group.[45] Pair interaction parameters were added between aromatic carbons and chain UA sites at least 5 bonds apart and between methylic and methylenic chain groups 6 bonds apart. Finally pair interaction parameters have been also added to describe the interaction between the $H_{2(n2)}$ and the methylenic group bonded to $C_{c1(*)}$ (see Table 5).

3.2. The FRM Approach. The interaction potential has been calculated with the FRM, which relies on the assumption that the interaction energy of a dimer can be approximated to a good accuracy as a sum of energy contributions between the pairs of fragments which concur to form both molecules. By

Table 4. BAB: Optimized Flexible Torsion Parameters

flexible torsions					
dihedral angle	n	k^d (kJ/mol)	dihedral angle	n	k^d (kJ/mol)
$C_3\widehat{C_4N}N_o$ (δ_1)	0	0.998	$(O)\widehat{NN_o}C_{n4}C_{n3}$ (δ_2)	0	1.997
	2	−5.739		2	−3.205
	4	0.174		4	0.502
	6	−0.047		6	−0.025
$C_{n2}\widehat{C_{n1}C_{c1}}\cdot C_{c2}$ (δ_3)	0	1.997	$C_2\widehat{C_1C_{c1}}C_{c2}$ (δ_5)	0	1.997
	2	1.358		2	1.358
	4	−0.325		4	−0.325
	6	−0.099		6	−0.099
$C_1\widehat{C_{c1}C_{c2}}C_{c2}$ (δ_6)	0	0.998	$C_{n1}\widehat{C_{c1}}\cdot C_{c2}C_{c2}$ (δ_4)	0	0.998
	1	3.657		1	3.657
	2	1.995		2	1.995
	3	7.504		3	7.504
	4	−0.263		4	−0.263
$C_{c3}\widehat{C_{c2}C_{c2}}C_{c1}\cdot$ (δ_7)	0	−2.106	$C_{c3}\widehat{C_{c2}C_{c2}}C_{c1}$ (δ_8)	0	−2.106
	1	4.330		1	4.330
	2	1.738		2	1.738
	3	7.520		3	7.520
	4	0.126		4	0.126
	5	0.172		5	0.172
	6	0.241		6	0.241

Table 5. Intramolecular LJ Parameters[a]

intramolecular LJ parameters		
site couple	σ (Å)	ε (kJ/mol)
$C_{c2}^{***} \cdots C_a$	3.30	0.69
$C_{c2}^{**} \cdots C_a$	3.56	0.69
$C_{c2}^{*} \cdots C_a$	3.56	0.69
$C_{c3} \cdots C_a$	3.56	0.69
$C_{c3} \cdots C_{c2}^{c1(*)}$	4.34	0.021
$C_{c2}^{c1(*)} \cdots H_{2(n2)}$	4.80	0.004

[a] C_a indicates an aromatic carbon site; C_{c2}^{*} is the C_{c2} site bonded to the C_{c3} one; C_{c2}^{**} and C_{c2}^{***} are the sites that follow along the aliphatic chain. Finally $C_{c2}^{c1(*)}$ represents the C_{c2} bonded to $C_{c1(*)}$.

must be verified that the electronic density on the *A* (*B*) moiety is as close as possible to that in the *AB* and *AH_a* molecules. This is of particular importance for the electronic density of the π orbitals in aromatic systems. Let us now consider a second molecule *CD* interacting with *AB* (of course *CD* can be the previous *AB* molecule moved to a different spatial location). A similar fragmentation scheme leads to

$$CD \simeq CH_c + H_dD - H_cH_d$$

The complete interaction energy af the *AB⋯CD* system can be recovered by summing up the interaction energy of all the involved pairs, including the fragments only formed by intruder atoms

$$
\begin{aligned}
E(AB\cdots CD) = \\
E(AH_a\cdots CH_c) + E(AH_a\cdots H_dD) - E(AH_a\cdots H_cH_d) + \\
E(H_bB\cdots CH_c) + E(H_bB\cdots H_dD) - E(H_bB\cdots H_cH_d) - \\
E(H_aH_b\cdots CH_c) - E(H_aH_b\cdots H_dD) + E(H_aH_b\cdots H_cH_d)
\end{aligned}
$$
(10)

The sign of each terms is determined by the single sign in the above fragmentation schemes for AB and CD. From the last equation, the computational advantage of the FRM approach is apparent: the interaction energy is written as a sum of interaction energies of pairs well smaller than the whole *AB⋯CD* system. For this calculation a suitable QM method able to recover a large part of the dispersion energy has to be employed. Since such QM methods scale at least as the fourth power of the number of electrons, the computational gain can be further appreciated. Previous applications of the FRM approach[17,35] have shown that, with a suitable choice of the method and basis set, a reliable database for many geometrical arrangements can be obtained and employed for FF parametrization.

3.3. Intermolecular Parametrization. The direct FRM route has been applied to the HAB molecule to sample its intermolecular PES, following the fragmentation scheme reported in Figure 3.

The reliability of the fragmentation using H_2 as intruder molecules was already validated.[35] Here, more attention has been paid to verify possible fragmentation schemes of the central aromatic core. With this aim preliminary calculations[46] have been performed on the HAB's smaller homologue, 4,4′-dimethylazoxybenzene. We found a cut along the $N-C_4$ bond (see Figure 1) preferable to that along N_O-C_{n4}, as the electronic density distribution of the resulting frag-

way of example, let us consider a simple *AB* molecule where *A* and *B* are two moieties connected by a single bond. The whole molecule can be formally written as

$$AB \simeq AH_a + H_bB - H_aH_b$$

where the two intruder atoms H_a and H_b are first included to saturate the *A* and *B* fragments and then removed as a H_aH_b molecule. The spatial position of the fragments is the same as in the whole molecule, whereas the location of the intruder atoms H_a and H_b is determined by the equilibrium geometry of the saturated fragments BH_a and H_bB, which normally correspond to stable molecules. For the success of the method it
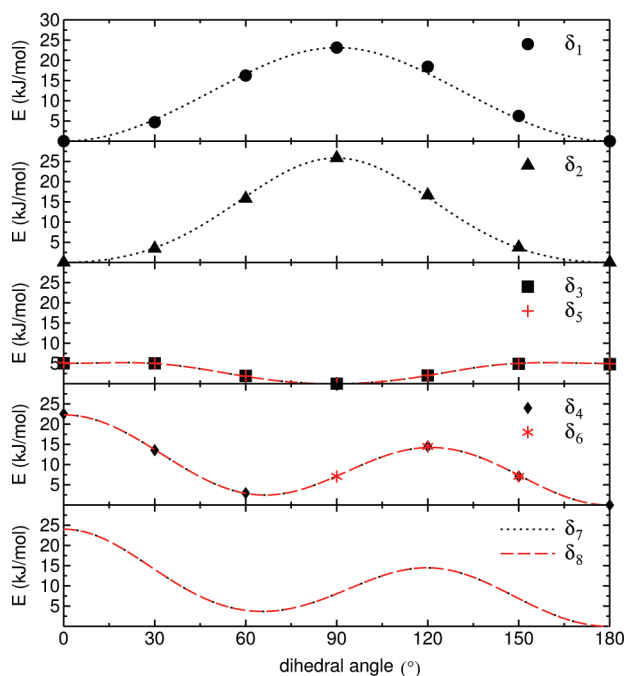

Figure 2. BAB (4,4′-dibutylazoxybenzene) - proper torsions, the symbols represent the sampled points while the dashed lines are the curves obtained with the model parametrized potential *V*. Only the region 0°–180° is shown because of symmetry reasons.

Force Fields for Mesogenic Molecules

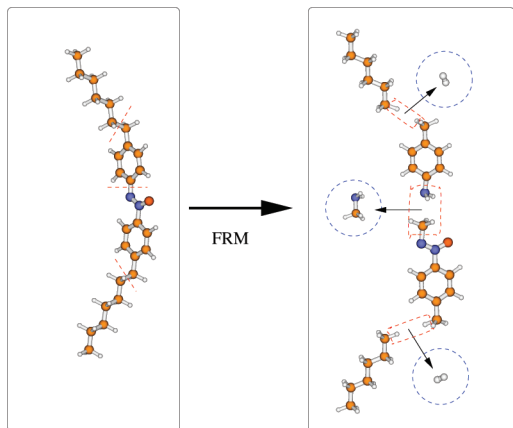*J. Chem. Theory Comput., Vol. 5, No. 7, 2009* **1871**

Figure 3. Fragmentation route for HAB. The fragmentation has been performed by cutting bonds as shown by the red dashed lines (left panel). The four resulting fragments are shown on the right, together with the intruder fragments, which are encircled in blue.
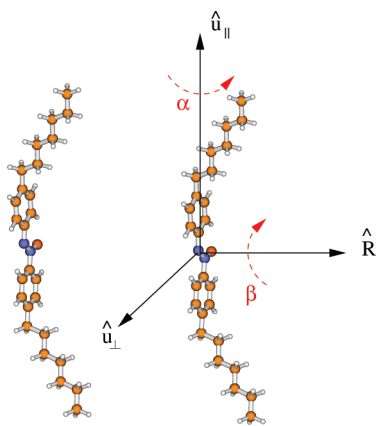

Figure 4. FRM sampling. Dimer arrangements are generated by displacing one HAB molecule with respect to the other by translation along $\hat{R}$, $\hat{u}_\perp$, or $\hat{u}_\parallel$ and/or rotation around α or β.

ments is more similar to that exhibited by the moieties in the whole molecule. Thus the final fragments are two hexanes, one 4-methylbenzenamine and one methyl,4-(methyl-NNO-azoxy)phenyl. It may be worth noting that the intruder molecule arising from the chosen scheme in the central core is a CH_3NH_2 molecule, as shown in Figure 3.

The low symmetry of the target dimer makes sampling the PES far from straightforward. However, a classification of the many dimer arrangements is still possible in terms of displacement vectors ($\hat{R}$, $\hat{u}_\perp$, and $\hat{u}_\parallel$) and Euler angles (α and β), as reported in Figure 4. Face-to-face (FF) configurations can be obtained by shifting one molecule along the vector $\hat{R}$, with $\alpha = 0°$ and $\beta = 0°$ or 180°. In the former case, the vectors N_O-O point in the same direction, and the geometries so obtained are labeled as parallel face-to-face (p-FF). In the latter, the vectors N_O-O point in opposite directions resulting in antiparallel (a-FF) arrangements. If both molecules are rotated by $\alpha = 90°$, the cores are found in a side-by-side disposition (p-SS or a-SS, whether $\beta = 0°$ or 180°). Side-to-face (p-SF and a-SF) geometries are obtained with a rotation of $\alpha = 90°$ of one molecule. If the β angle is set to 90°, the two cores draw a cross and the x-FF, x-SF, and x-SS arrangements can be created by applying a further

rotation around the β-rotated long molecular axis of 0°, 90° on one or both molecules, respectively. Finally if one molecule is rotated around $\hat{u}_\perp$, the dimer is found in a T-shaped (TS) configuration.

Further subclasses can be created by exploiting the relative position of the side chains of the two dimer molecules. If the symbol " $\subset$ " is used to sketch the HAB molecule, three subclasses can be determined depending on when the alkyl chains point in the same direction ($\subset \subset$), toward each other ($\subset \supset$), or in opposite directions ($\supset \subset$).

The PES sampling has been performed by computing the FRM energy of $N_{geom} \sim 2000$ geometries (see eq 5).

From a preliminary analysis of the resulting FRM database, the configurations with the more attractive interactions are the $\supset \subset$ ones, where the steric chain repulsion effect does not prevent the rings and the NNO group to reach their most favorable positions with respect of the same groups of the other molecule. For the same reason, less attractive energies are found for the $\subset \subset$ and $\subset \supset$ arrangements, in this order.

In the latter, the steric effect dominates and the interaction energy wells are far less deep and shifted to higher values of the displacement coordinate. For example, for the p-FF case, reported in Figure 5, $\supset \subset$ have a maximum interaction energy of about −50 kJ/mol, $\subset \subset$ reach −20 kJ/mol at most, and $\subset \supset$ only are −5 kJ/mol. The situation is similar for the a-FF geometry: here the $\supset \subset$ is even more the favorite since the oxygens point in opposite directions and the maximum interaction energy can reach −57 kJ/mol.

Among all classes, the most favored geometries are p-FF, a-FF, and x-FF configurations, where the aromatic rings come closer to each other and the interaction π energy significantly contributes to the total interaction energy.[22,36] It may be worth noting that in the x-FF case, the aliphatic chains are not superimposed in any geometry with the result that their repulsion effect is not as important as in the previous configurations. This means that $\subset \subset$, $\subset \supset$, and $\supset \subset$ geometries have similar situations, with −40 kJ/mol maximum interaction energies in all cases. The interaction energies for the SS configurations are less attractive: the a-SS geometries do not reach −30 kJ/mol and p-SS ones arrive at −18 kJ/mol, at most. Furthermore, p-SF does not overstep the −20 kJ/mol, showing energies between the FF case and the SS one. Also the x-SF configurations are less energetic than the x-FF (−25 kJ/mol and −40 kJ/mol, respectively). Finally TS arrangements present maximum interaction energy of about −12 kJ/mol. As far as the contact distance is concerned, it can be noted that, again, there are three different kinds of disposition: p-FF, a-FF, and x-FF configurations have a contact distance of about 3 Å, p-SS and a-SS of 6 Å, and TS above 8 Å. From this first picture, the anisotropic nature of the HAB molecule shows up clearly. This is a well-known feature of many calamitic LC, as for instance the nCB series:[47] the contact distance and the well depths of all interaction curves strongly depend on the monomer relative orientations.

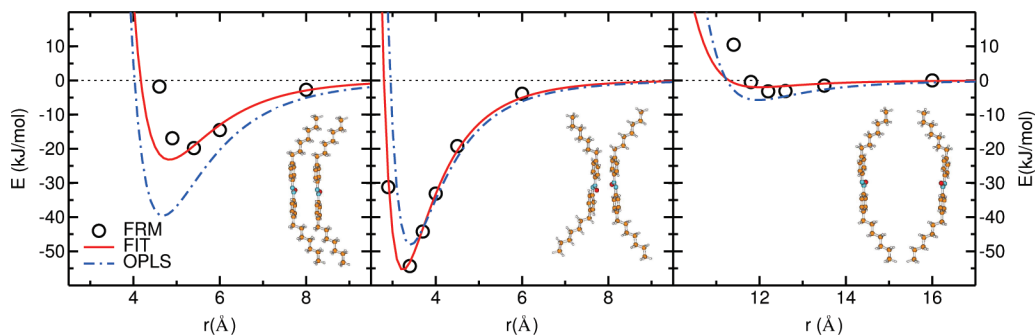All the sampled energies have been fitted by means of functional (5) with the model described in Figure 1. Equivalent sites have been given the same σ, ε, and q values.

Figure 5. HAB computed and fitted energy curves for selected geometrical arrangements: p-FF ⊂ ⊂, p-FF ⊃ ⊂, and p-FF ⊂ ⊃. The points represent the FRM energies and the solid lines the fitted energies. OPLS predictions are also reported with dashed blue lines for comparison.

Table 6. HAB: Optimized Intermolecular Parameters

site	ε (kJ/mol)	σ (Å)	q (e)	site	ε (kJ/mol)	σ (Å)	q (e)
$C_{c1(*)}$	0.148	4.15	0.272	C_{n4}	3.402	2.69	−0.047
C_1	1.878	2.79	−0.367	C_{n3}	0.664	3.10	−0.126
C_2	0.145	3.52	−0.043	C_{n2}	0.066	4.20	−0.066
C_3	1.076	3.38	−0.043	C_{n1}	1.652	2.00	−0.050
C_4	2.632	2.00	0.098	H_{n3}	0.082	2.00	0.093
H_2	0.023	2.48	0.082	H_{n2}	0.053	2.00	0.119
H_3	0.074	2.35	0.048	C_{c1}	2.590	3.44	−0.009
N	1.135	3.05	−0.374	C_{c2}	0.246	4.10	0.000
N_O	0.020	3.82	0.729	C_{c3}	0.020	3.70	0.000
O	0.180	3.03	−0.428				

No other constraints were imposed but for σ and q of the methylene (C_{c2}) groups of the chains. These sites have been assumed chargeless as in previuos applications,[17,35] since this allows a straightfoward extension of the FF to higher homologues (see the nCB series[48]). As to the $\sigma_{C_{c2}}$ parameter, a first fitting yielded a standard deviation of 2.22 kJ/mol, with a value (4.4 Å) significantly larger than that obtained for butane (3.905 Å[49]) or 5OCB (3.76 Å[17]). With this set of parameters, a preliminary MD run, performed in the NPT ensemble on an isotropic system of 64 HAB molecule at 1 atm and 370 K gave a density underestimated by ∼4% with respect to the experimental value. However, another fit with $\sigma_{C_{c2}}$ reduced to 4.1 Å, and a slightly larger standard deviation (2.48 kJ/mol) yielded a density within 1% of the experimental data.

The final optimized parameter set that corresponds to this fit can be seen in Table 6.

In Figures 5 and 6, the energies obtained with the FRM are compared with those predicted by the OPLS[21,49] empirical force field, widely employed in simulations of the liquid phase of many smaller molecules. The OPLS-FF describes the FRM energy surface with a standard deviation of 9.56 kJ/mol. This can be seen as a remarkable achievement, and a proof of the good transferability of the OPLS parameters. However, the extreme sensitivity of the properties of liquid crystalline materials to even minor changes of the molecular structures and interactions supports the need for a more accurate representation of the FRM PES, as attained by our fitting procedure, which leads to the standard deviation of 2.48 kJ/mol. (See also Figures 5 and 6 for a visual estimate of the agreement at a few selected configurations.) The need for an accurate description of the PES is also apparent if we consider that the FRM approach is able to reproduce the interaction energies of HAB dimers with great accuracy, as

Figure 6 shows. In each panel of this figure we include a point (labeled DIMER) that corresponds to the true *ab initio* interaction energy of the dimer in that configuration, i.e. the value obtained without decomposing the molecule as in the FRM scheme. The results of Figure 6 prove two things: i) that the FRM gives an excellent agreement with the true value of the interaction energy (e.g., −17.1 vs −16.9 kJ/ mol with the FRM for the p-FF arrangement) and ii) that the fit we employ faithfully describes the PES we sampled.

As a test of the predictive capability of the ABD-FF, the energy curves of unsampled geometries have been calculated both with the model function and using FRM. The results are reported in Figure 7, together with the OPLS predictions. In the top panel an energy curve for a β rotation is shown. One HAB molecule was also translated by 2 Å along $\hat{u}_{\perp}$, 3.5 Å along $\hat{R}$ and rotated by α = 180°. Here, both curves are in good agreement with the FRM points.

The central panel shows an interaction energy curve, obtained by displacing one molecule along the $u_{\|}$ direction, with a shift of 2.5 Å along $\hat{u}_{\perp}$, 4.0 Å along $\hat{R}$, and a rotation of α = 40° and β = 50°. In this case the fitted curve traces out the FRM point positions better than the OPLS. Finally, in the third panel, a similar curve is reported for a a-FF ⊃ ⊂ type, again obtained by displacing the second molecule along $u_{\|}$ after a translation of 3.4 Å along $\hat{R}$ and a 180° rotation of both α and β. Even if the OPLS prediction is not so far from the FRM points, the fitted curves are significantly closer to the FRM data.

3.4. Preliminary MD Results. MD simulations have been carried out on condensed phases of HAB in the NPT and NVE ensembles. The first type of conditions were used when searching for the transition temperatures, while the latter have been adopted for the calculation of dynamic properties. In all cases, we have used the largest number of molecules we could afford with a cubic box, to prevent any artificial ordering of the sample, induced e.g. by an elongated box.

210 HAB molecules have been considered a sensible starting point, mainly for the simulation of the isotropic phase. However, a larger system of 600 molecules (corresponding to 22200 interaction sites) has been adopted to study the ordered phases and to evaluate the system size effect on the results.

The isotropic phase has been obtained starting from a 6 × 7 × 5 cubic lattice disposition where the HAB centers of mass were placed on the nodes, with the long molecular axis

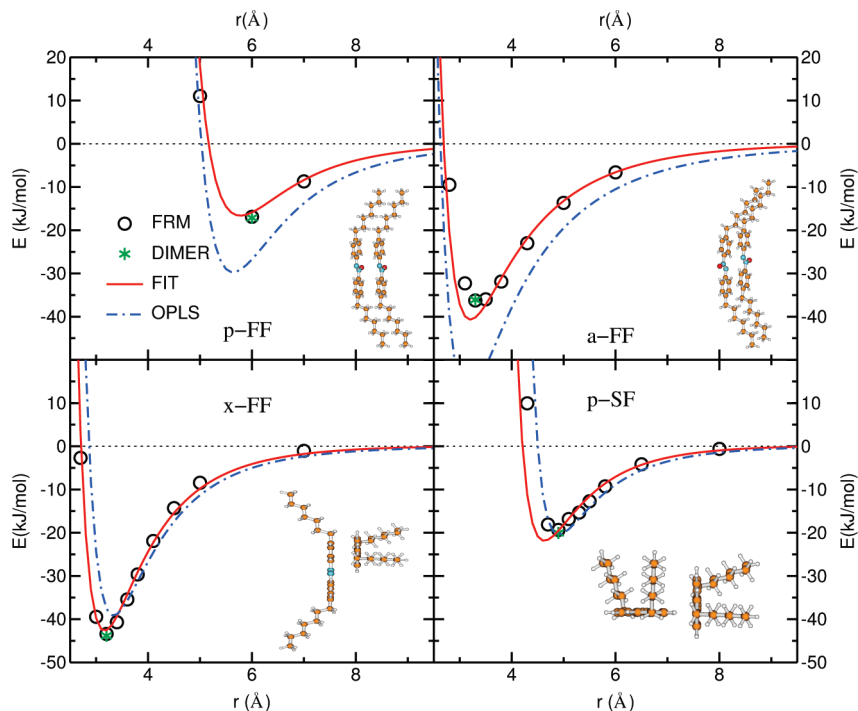Force Fields for Mesogenic Molecules

J. Chem. Theory Comput., Vol. 5, No. 7, 2009 **1873**

Figure 6. HAB computed and fitted energy curves for selected geometrical arrangements: p-FF ⊂ ⊂, a-FF ⊂ ⊂, x-FF ⊃ ⊂, and p-SF ⊃ ⊂. In the first two geometries, a shift of −2 Å was applied along $\hat{u}_\perp$. The points represent the FRM energies and the solid lines the fitted energies. The green point marked 'DIMER' in each panel shows the interaction energy of the dimer, computed *ab initio* for the *whole* molecules (no FRM, see text). OPLS predictions are also reported with dashed blue lines for comparison.
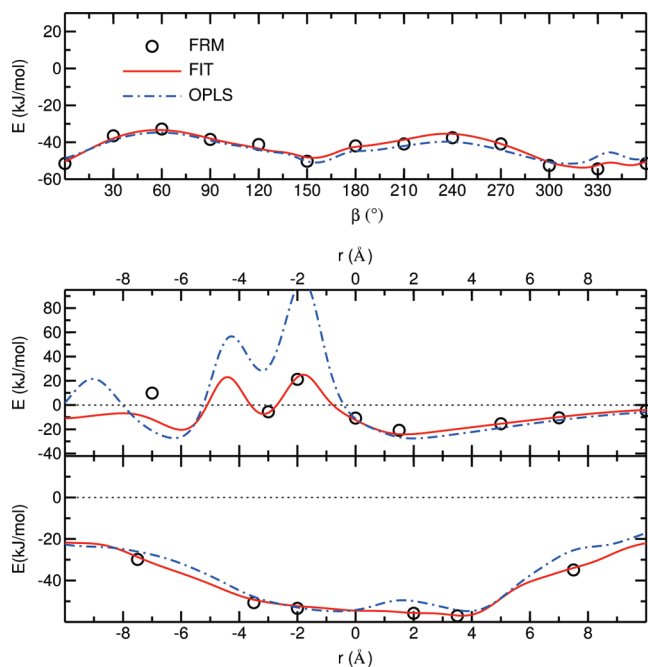

Figure 7. HAB interaction energy predicted by the fitting function (solid line) and control FRM values (open circles). The OPLS prediction is also shown (dashed line).

Figure 8. Time evolution of orientational, P_2, and positional, τ, order parameter at three temperatures for the system with 600 molecules. Horizontal dashed lines represent the conventional orientational and positional order threshold.

aligned along one of the box axes ($\hat{z}$). The system has been equilibrated in the NPT ensemble at 400 K for 5 ns and then cooled at 380 K and in successive steps at 370 K, 350 K, 330 K, and 300 K. Given that the experimental[50] nematic−isotropic transition takes place at 342 K, the temperatures relevant for the true isotropic phase are 350 and 370 K.
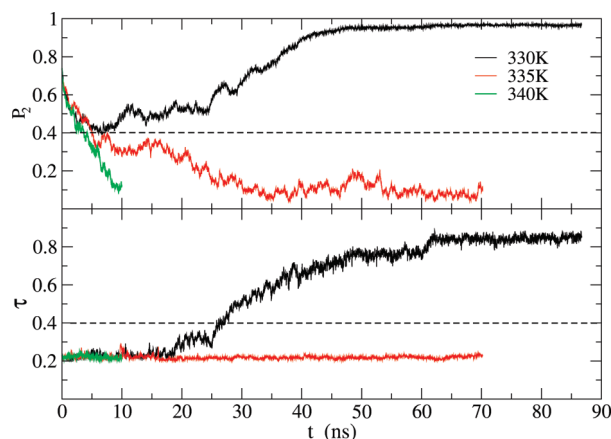
The system of 600 molecules was obtained from a lattice structure in a cubic box at low density which was later compressed to the isotropic liquid density.

After equilibration, an orienting field was applied for 0.5 ns under NPT conditions ($T = 340$ K). The field was able to produce a P_2 value of 0.74 with no positional order. Later, the field was switched off, and this metastable state was used as a common starting configuration for three runs at 340, 335, and 330 K.

The evolution of the orientational and positional order parameter was then followed for some tens ns, with the results shown in Figure 8. These data show clearly the
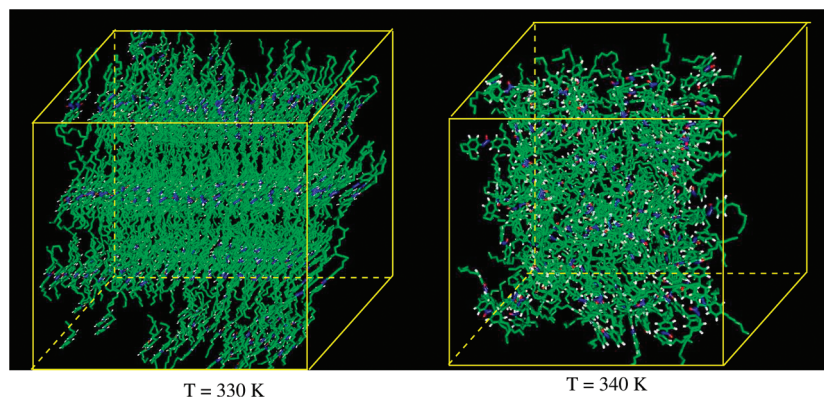
Figure 9. Snapshots of the smectic (left, $T = 330$ K, 600 molecules) and isotropic (right, $T = 340$ K, 210 molecules) phases of the simulated HAB systems.

Table 7. Experimental and Simulated Results of Density and Translational Diffusion Coefficient in the Isotropic Phase[a]

T (K)	ρ_{exp}[b] (g/cm^3)	ρ_{MD}^{NPT} (g/cm^3)	T_{NVE} (K)	ρ_{MD}^{NVE} (g/cm^3)	D_{exp}[b] (10^{-10} m^2/s)	D_{MD} (10^{-10} m^2/s)
300	1.002	–	302.0	0.972	0.27	0.23 ± 0.01
330	0.964	–	330.4	0.947	0.80	1.04 ± 0.04
350	0.939	0.930 ± 0.004	353.0	0.931	1.71	1.82 ± 0.06
370	0.915	0.914 ± 0.004	373.5	0.913	3.10	3.05 ± 0.01
380	0.902	0.906 ± 0.003	–	–	–	–
400	0.877	0.889 ± 0.003	–	–	–	–

[a] At $T = 300$ K and $T = 330$ K ρ_{exp} means the density of the supercooled isotropic phase, *i.e.* that extrapolated from experimental densities in the isotropic range, while D has been obtained from a geometric average of the longitudinal and transverse diffusion coefficients. [b] Reference 25.

Figure 10. Time dependence of the MSD in the normal and supercooled isotropic phase (log−log scale).

existence of a smectic phase at 330 K and an isotropic phase at 335 and 340 K. This might indicate that our model does not lead to the nematic phase of HAB. However, it must be stressed that reproducing by atomistic simulation a phase that spans a range of temperature of just $\simeq 10$ K is a formidable challenge.[15]

As to the smectic phase, our analysis finds an interlayer spacing of $\simeq 22.5$ Å, significantly smaller than the experimental value of 28.9 Å,[51] that corresponds to a tilt angle of $\simeq 18°$ and identifies a smectic A phase. As a consequence it is likely that our system is not arranged in a smectic A phase. However, it is certainly encouraging to observe a spontaneous positional reordering at a temperature just above the experimental smectic-nematic transition temperature (327 K).[50] The layered structure of the smectic phase is apparent in the left panel of Figure 9, while the right panel shows a snapshot of the isotropic phase.

In the case of the isotropic phase, the MD density values at constant atmospheric pressure are in very good agreement with the experimental data,[50] with errors always below 1% (see Table 7). It is worth noticing that a good reproduction of density is essential, not only for a correct description of the structure of the system but also for an accurate evaluation of dynamic properties, e.g. diffusion, which is extremely sensitive to the density in these materials.

Translational diffusion has been evaluated from trajectories obtained in NVE runs, at four different temperatures in the isotropic phase. The same data have also been used for a collective dynamical property, namely shear viscosity.
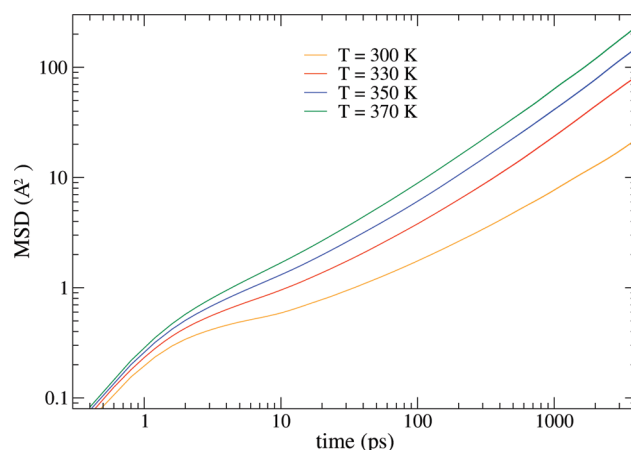
As far as diffusion is concerned, for all trajectories the MSDs were computed according to eq 8 using a 4 ns correlation time window, and the curves are reported in Figure 10.

The computed translational diffusion coefficient is reported in Table 7 together with its experimental counterpart,[25] which is reproduced to a good extent. The Arrhenius treatment of the temperature dependence of D leads to an activation energy of 33.4 KJ/mol, also in good agreement with the experimental data of 31.9 KJ/mol.[25] Upon supercooling the isotropic system down to 330 and 300 K, a subdiffusive behavior becomes apparent, with the β relaxation regime plateau between 1 and 10 ps.[52] This is the same time window already found in a previous work on supercooled isotropic mesogens,[53,54] so it may be considered a fairly general feature of this kind of materials.

Shear viscosity, η_s, for the isotropic phase has been investigated, too. This is a collective property that can only be averaged on successive time origins: as a consequence, it is affected by larger statistical uncertainty, and much longer simulations are needed to obtain reliable values for the long time limit of the function $C_\sigma(t)$ of eq 9. To some extent, the situation can be improved fitting the curves with a double exponential function, as done elsewhere.[24] In Figure 11 the integral, whose infinite time limit yields η_s, is reported vs time, together with the fitting curves, where a fitting window of 0−400 ps has been used at all temperatures.

Force Fields for Mesogenic Molecules

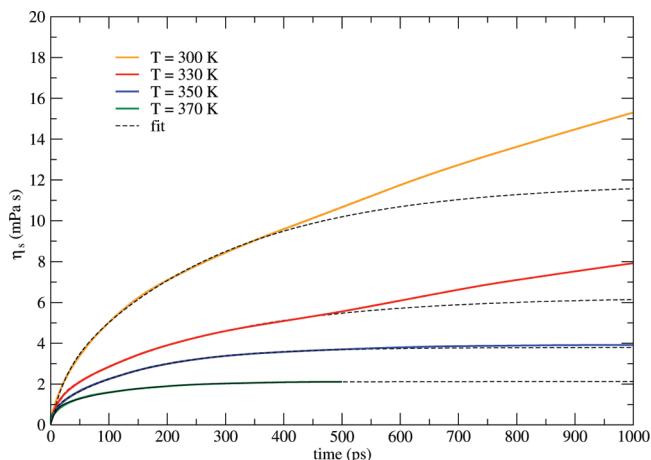*J. Chem. Theory Comput., Vol. 5, No. 7, 2009* **1875**

Figure 11. Calculation of HAB shear viscosity at different temperatures for the isotropic phase, according to eq 9. The exponential fits are reported in dashed lines.

Table 8. Temperature Dependence of Shear Viscosity in the Normal and Supercooled Isotropic Phase

T (K)	η_s^{MD} (mPa s)
300.2	11.9
330.4	6.3
353.0	3.8
373.5	2.1

Unfortunately, experimental data are not available for HAB viscosity, as far as we know, so we can try to estimate our MD results by comparison with the corresponding experimental data for the nCB series. $T = 353$ K corresponds roughly to a reduced temperature of 1.05, where HAB shows (see Table 8) $\eta_s = 3.8$ mPa s, while experimental values for the nCB series oscillate between 10 and 20 mPa s (see ref 24 and references therein). Assuming[55] an inverse relationship between D and η_s, the experimental D value for HAB (1.71), compared to that of nCB series (0.60–1.0 (10^{-10} m^2/s)[24]), would yield a viscosity value in the range 5–10 mPa s, slightly larger than our computed value. However, only experimental data can definitely assess the accuracy of the MD results.

4. Conclusions

The FRM approach to force fields has been applied to HAB in the direct scheme of implementation. Compared to the indirect scheme adopted in the first application of FRM to mesogens (the series of nCB[23,24]), the direct one turned out to provide more accurate results of key quantities for the description of condensed phase behavior, e.g. density and diffusion coefficient of 5OCB.[17] In the present study of HAB, the density of the isotropic phase is reproduced within 1% of the experimental value, and also a basic probe of dynamics, i.e. the diffusion coefficient D, agrees quite satisfactorily with the measured data. The success obtained with density and D supports some confidence that the MD results of shear viscosity also may be close to that of the real system, which are not available, to our knowledge.

In addition to the isotropic phase, that appears faithfully modeled, we have obtained a smectic phase at 330 K. It is

rewarding that this smectic phase develops with a spontaneous positional reordering from a system with a P_2 as low as 0.4 and essentially no positional order. This locates the transition temperature to the isotropic phase between 330 and 340 K, i.e. within 10 K of the measured value of 342 K. However, from the data collected so far, the positionally ordered phase seems a SmC, instead of the SmA formed by the real system. More importantly, we have been unable to obtain a nematic phase with the present parametrization of the force field.

The incorrect smectic obtained and the missing nematic phase indicate that some changes are to made on our model. We are currently focusing on two main issues. The first improvement would entail abandoning the hybrid model adopted so far (the hydrogens of the alkyl chains are fused to the carbon they are linked to). At a significant increase of the number of interaction sites and hence computational time, a truly full atomic model should be able to better match the *ab initio* PES, maybe resorting to the exp-6 potential instead of the less flexible LJ. In turn, this would reduce distorsions that might affect some dimer configurations and propagate into an incorrect modeling of the phase diagram of the system, given the well-known sensitivity of these materials to apparently minor variations of the molecular structure and interactions.

The second point to address regards the selection of configurations whose interaction energy is to be *ab initio* calculated. We plan to combine chemical intuition with short MD runs, from which significant dimer and trimer configurations could be extracted. This way, the extent of nonadditivity could be evaluated and the database of dimer arrangements increased in a more physically driven approach.

References

(1) Allen, M. P.; Tildesley, D. J. *Computer Simulation of Liquids*; Clarendon: Oxford, 1987.

(2) Frenkel, D.; Smith, B. *Understanding Molecular Simulations;* Academic Press: San Diego, 1996.

(3) *Advances in the Computer Simulations of Liquid Crystals NATO ASI series*; Pasini, P., Zannoni, C., Eds.; Kluwer: Dordrecht, 2000.

(4) Kremer, K. *Macromol. Chem. Phys.* **2003**, *204*, 257.

(5) *Computer Simulations of Liquid Crystals and Polymers NATO ASI series*; Pasini, P., Zannoni, C., Zumer, S., Eds.; Kluwer: Dordrecht, 2005.

(6) Care, C. M.; Cleaver, D. J. *Rep. Prog. Phys.* **2005**, *68*, 2665.

(7) Amovilli, A.; Cacelli, I.; Cinacchi, G.; De Gaetani, L.; Prampolini, G.; Tani, A. *Theor. Chim. Acc.* **2007**, *117*, 885.

(8) Maple, J. R.; Dinur, U.; Hagler, A. T. *Proc. Natl. Acad. Sci. U. S. A.* **1988**, *85*, 5350.

(9) Dasgupta, S.; Yamasaki, T.; Goddard, W. A., III *J. Chem. Phys.* **1996**, *104*, 2898.

(10) Palmo, K.; Mannfors, B.; Mirkin, N. G.; Krimm, S. *Biopolymers* **2003**, *68*, 383.

(11) Maple, J. R.; Hwang, M.-J.; Stockfish, T. P.; Dinur, U.; Waldman, M.; Ewig, C. S.; Hagler, A. T. *J. Comput. Chem.* **1994**, *15*, 162.

(12) Halgren, T. A. *J. Comput. Chem.* **1996**, *17*, 490.

(13) Yang, L.; Tan, C.; Hsieh, M.; Wang, J.; Duan, Y.; Cieplak, P.; Caldwell, J.; Kollmann, P. A.; Luo, R. *J. Phys. Chem. B* **2006**, *110*, 13166.

(14) Wang, J. M.; Wolf, R. M.; Caldwell, J. W.; Kollman, P. A.; Case, D. A. *J. Comput. Chem.* **2004**, *25*, 1157.

(15) Bockmann, M.; Peter, C.; Delle Site, L.; Doltsinis, N.; Kremer, K.; Marx, D. *J. Chem. Theory Comput.* **2007**, *3*, 1789.

(16) Cacelli, I.; Prampolini, G. JOYCE is free software, available under the terms of the GNU License at http://tglc.dcci.unipi.it/ Pisa (Italy) 2007.

(17) Cacelli, I.; Lami, C.; Prampolini, G. *J. Comput. Chem.* **2009**, *30*, 366.

(18) Wang, L.; Sadus, R. *J. Chem. Phys.* **2006**, *125*, 074503.

(19) Tiberio, G.; Muccioli, L.; Berardi, R.; Zannoni, C. *ChemPhysChem* **2009**, *10*, 125.

(20) Cacelli, I.; Cinacchi, G.; Prampolini, G.; Tani, A. *J. Am. Chem. Soc.* **2004**, *126*, 14278.

(21) Jorgensen, W. L.; Severance, D. L. *J. Am. Chem. Soc.* **1990**, *112*, 4768.

(22) Amovilli, C.; Cacelli, I.; Campanile, S.; Prampolini, G. *J. Chem. Phys.* **2002**, *117*, 3003.

(23) Cacelli, I.; Prampolini, G.; Tani, A. *J. Phys. Chem. B* **2005**, *109*, 3531.

(24) Cifelli, M.; De Gaetani, L.; Prampolini, G.; Tani, A. *J. Phys. Chem. B* **2008**, *112*, 9777.

(25) Cifelli, M.; Cinacchi, G.; De Gaetani, L. *J. Chem. Phys.* **2006**, *125*, 164912.

(26) Frisch, M. J.; Trucks, G. W.; Schlegel, H. B.; Scuseria, G. E.; Robb, M. A.; Cheeseman, J. R.; Montgomery, J. A., Jr.; Vreven, T.; Kudin, K. N.; Burant, J. C.; Millam, J. M.; Iyengar, S. S.; Tomasi, J.; Barone, V.; Mennucci, B.; Cossi, M.; Scalmani, G.; Rega, N.; Petersson, G. A.; Nakatsuji, H.; Hada, M.; Ehara, M.; Toyota, K.; Fukuda, R.; Hasegawa, J.; Ishida, M.; Nakajima, T.; Honda, Y.; Kitao, O.; Nakai, H.; Klene, M.; Li, X.; Knox, J. E.; Hratchian, H. P.; Cross, J. B.; Bakken, V.; Adamo, C.; Jaramillo, J.; Gomperts, R.; Stratmann, R. E.; Yazyev, O.; Austin, A. J.; Cammi, R.; Pomelli, C.; Ochterski, J. W.; Ayala, P. Y.; Morokuma, K.; Voth, G. A.; Salvador, P.; Dannenberg, J. J.; Zakrzewski, V. G.; Dapprich, S.; Daniels, A. D.; Strain, M. C.; Farkas, O.; Malick, D. K.; Rabuck, A. D.; Raghavachari, K.; Foresman, J. B.; Ortiz, J. V.; Cui, Q.; Baboul, A. G.; Clifford, S.; Cioslowski, J.; Stefanov, B. B.; Liu, G.; Liashenko, A.; Piskorz, P.; Komaromi, I.; Martin, R. L.; Fox, D. J.; Keith, T.; Al-Laham, M. A.; Peng, C. Y.; Nanayakkara, A.; Challacombe, M.; Gill, P. M. W.; Johnson, B.; Chen, W.; Wong, M. W.; Gonzalez, C.; Pople, J. A. *Gaussian 03, Revision C.02*; Gaussian, Inc.: Wallingford, CT, 2004.

(27) Becke, A. D. *J. Chem. Phys.* **1993**, *98*, 5648.

(28) Cacelli, I.; Prampolini, G. *J. Chem. Theory Comput.* **2007**, *3*, 1803.

(29) Boys, S. F.; Bernardi, F. *Mol. Phys.* **1970**, *19*, 553.

(30) Hobza, P.; Selzle, H. L.; Schlag, E. W. *J. Phys. Chem.* **1996**, *100*, 18790.

(31) Hobza, P.; Zahradník, R.; Müller-Dethlefs, K. *Collect. Czech. Chem. Commun.* **2006**, *71*, 443.

(32) Tsuzuki, S.; Honda, K.; Uchimaru, T.; Mikami, M.; Tanabe, K. *J. Am. Chem. Soc.* **2002**, *124*, 104.

(33) Sinnokrot, M. O.; Sherrill, C. D. *J. Phys. Chem. A* **2006**, *110*, 10656.

(34) Cacelli, I.; Cinacchi, G.; Geloni, C.; Prampolini, G.; Tani, A. *Mol. Cryst. Liq. Cryst.* **2003**, *395*, 171.

(35) Bizzarri, M.; Cacelli, I.; Prampolini, G.; Tani, A. *J. Phys. Chem. A* **2004**, *108*, 10336.

(36) Prampolini, G. *J. Chem. Theory Comput.* **2006**, *2*, 556.

(37) Paschen, D.; Geiger, A. *MOSCITO 3.9*; Department of Physical Chemistry, University of Dortmund: 2000.

(38) Ryckaert, J. P.; Ciccotti, G.; Berendsen, H. J. C. *J. Comput. Phys.* **1977**, *55*, 3336.

(39) Darden, T. A.; York, D.; Pedersen, L. *J. Chem. Phys.* **1993**, *98*, 10089.

(40) Essmann, U.; Perera, L.; Berkowitz, M. L.; Darden, A.; Lee, H.; Pedersen, L. *J. Chem. Phys.* **1995**, *103*, 8577.

(41) Berendsen, H. J. C.; Postma, J. P. M.; van Gusteren, W. F.; Di Nola, A.; Haak, J. R. *J. Chem. Phys.* **1984**, *81*, 3684.

(42) Bates, M. A.; Luckhurst, G. R. *J. Chem. Phys.* **1999**, *110*, 7087.

(43) Hansen, J. P.; McDonald, I. R. *Theory of Simple Liquids*; Academic Press: New York, 1986.

(44) Cinacchi, G.; Prampolini, G. *J. Phys. Chem. A* **2003**, *107*, 5228.

(45) Tsuzuki, S.; Honda, K.; Uchimaru, T.; Mikami, M.; Tanabe, K. *J. Am. Chem. Soc.* **2000**, *122*, 3746.

(46) Cimoli, A. *Tesi di Laurea*; Università di Pisa, Pisa (Italy), 2007.

(47) Cacelli, I.; De Gaetani, L.; Prampolini, G.; Tani, A. *Mol. Cryst. Liq. Cryst.* **2007**, *465*, 175.

(48) Cacelli, I.; De Gaetani, L.; Prampolini, G.; Tani, A. *J. Phys. Chem. B* **2007**, *111*, 2130.

(49) Jorgensen, W.; Laird, E.; Nguyen, T.; Tirado-Rives, J. *J. Comput. Chem.* **1993**, *14*, 206.

(50) Jagadeesh, B.; Prabhakar, A.; Rao, M. H. V. R.; Murty, C. V. S.; Pisipati, V. G. K. M.; Kunwar, A. C.; Bowers, C. R. *J. Phys. Chem. B* **2004**, *108*, 11272.

(51) Pape, E. *Mol. Cryst. Liq. Cryst.* **1984**, *102*, 271.

(52) Götze, W.; Sjögren, L. *Rep. Prog. Phys.* **1992**, *55*, 241.

(53) De Gaetani, L.; Prampolini, G.; Tani, A. *J. Phys. Chem. B* **2007**, *111*, 7473.

(54) De Gaetani, L.; Prampolini, G.; Tani, A. *J. Chem. Phys.* **2008**, *128*, 194501.

(55) Hansen, J. P.; McDonald, I. R. *Theory of Simple Liquids*; Academic Press: New York, 1986.